Nonlinear interactions of dipolar excitons and polaritons in MoS_2 bilayers

Charalambos Louca,[1,*] Armando Genco,[2,†] Salvatore Chiavazzo,[3] Thomas P. Lyons,[1,4] Sam Randerson,[1] Chiara Trovatello,[2] Peter Claronino,[1] Rahul Jayaprakash,[1] Kenji Watanabe,[5] Takashi Taniguchi,[5] Stefano Dal Conte,[2] David G. Lidzey,[1] Giulio Cerullo,[2] Oleksandr Kyriienko,[3] and Alexander I. Tartakovskii[1,‡]

[1]*Department of Physics and Astronomy, The University of Sheffield, Sheffield S3 7RH, UK*

[2]*Dipartimento di Fisica, Politecnico di Milano, Piazza Leonardo da Vinci, 32, Milano, 20133, Italy*

[3]*Department of Physics, University of Exeter, Stocker Road, Exeter, EX4 4PY, UK*

[4]*RIKEN Center for Emergent Matter Science, Wako, Saitama, 351-0198, Japan*

[5]*Advanced Materials Laboratory, National Institute for Materials Science, 1-1 Namiki, Tsukuba, 305-0044, Japan*

Nonlinear interactions between excitons strongly coupled to light are key for accessing quantum many-body phenomena in polariton systems[1–5]. Atomically-thin two-dimensional semiconductors provide an attractive platform for strong light-matter coupling owing to many controllable excitonic degrees of freedom[6–10]. Among these, the recently emerged exciton hybridization opens access to unexplored excitonic species [11–13, 15, 16], with a promise of enhanced interactions[14]. Here, we employ hybridized interlayer excitons (hIX) in bilayer MoS_2 [11, 12, 15, 16] to achieve highly nonlinear excitonic and polaritonic effects. Such interlayer excitons possess an out-of-plane electric dipole [11] as well as an unusually large oscillator strength [12] allowing observation of dipolar polaritons (dipolaritons [17–19]) in bilayers in optical microcavities. Compared to excitons and polaritons in MoS_2 monolayers, both hIX and dipolaritons exhibit ≈ 8 times higher nonlinearity, which is further strongly enhanced

when hIX and intralayer excitons, sharing the same valence band, are excited simultaneously. This gives rise to a highly nonlinear regime which we describe theoretically by introducing a concept of hole crowding. The presented insight into many-body interactions provides new tools for accessing few-polariton quantum correlations [20–22].

Excitons in two-dimensional transition metal dichalcogenides (TMDs) have large oscillator strengths and binding energies [23], making them attractive as a platform for studies of strong light-matter coupling in optical microcavities [6–9]. A variety of polaritonic states have been realised using monolayers of MX_2 (M=Mo, W; X=S, Se) embedded in tunable [7, 9, 10, 24] and monolithic microcavities [14, 25–28].

One of the central research themes in polaritonics is the study of nonlinear interactions leading to extremely rich phenomena such as Bose-Einstein condensation [1, 2], polariton lasing [3, 4] or optical parametric amplification [5]. Polaritons formed from tightly bound neutral intralayer excitons in TMDs are not expected to show strong nonlinearity. However, pronounced nonlinear behavior was observed for trion polaritons [24, 29] and Rydberg polaritons [30]. Enhanced nonlinearity can be achieved by employing excitonic states with a physically separated electron and hole, e.g. in adjacent atomic layers [31] or quantum wells [17–19, 32, 33]. Such interlayer excitons have a large out-of-plane electric dipole moment, and thus can strongly mutually interact [34]. Typically, however, interlayer or 'spatially indirect' excitons possess low oscillator strength [31, 35]. Thus, in order to strongly couple to cavity photons, hybridization with high-oscillator-strength intralayer excitons is required [14, 17–19, 36].

An attractive approach for realization of dipolar excitons and polaritons is to employ the recently discovered exciton hybridization in MoS_2 bilayers [12, 37]. This

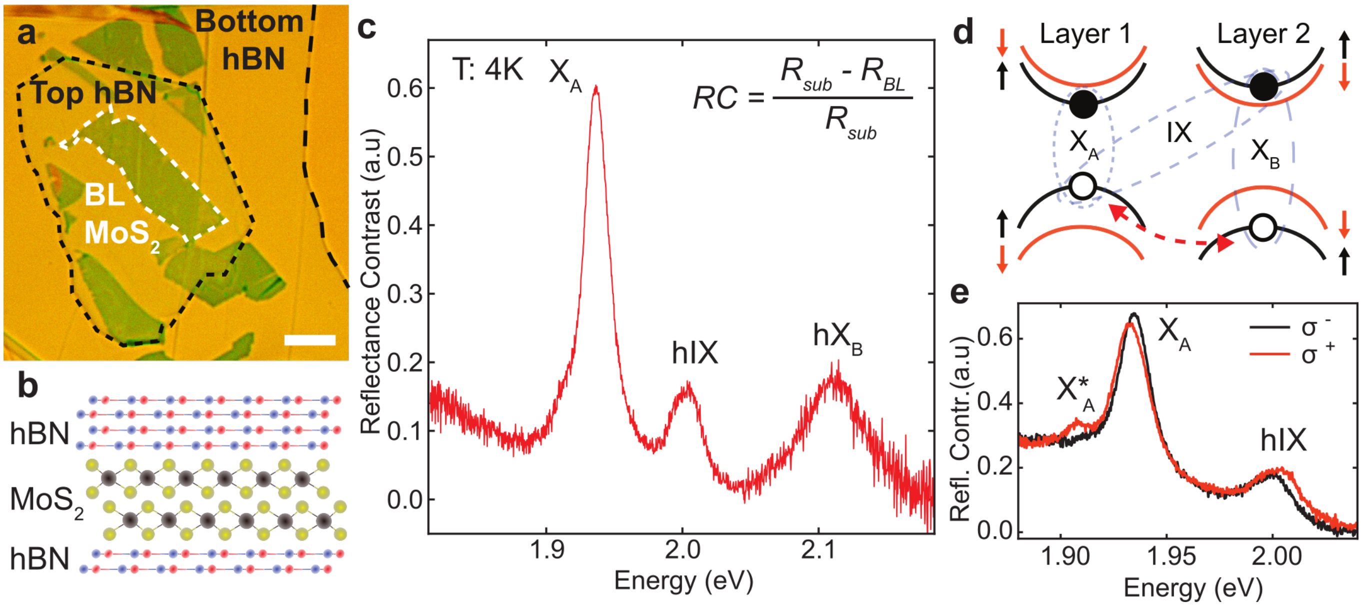

FIG. 1. **Homobilayer MoS_2 and its optical response. a,** Bright field microscope image of an encapsulated BL MoS_2 transferred on top of a DBR. Scale bar: 10 μm. **b,** Schematic side-view of the fabricated heterostructure comprising a BL MoS_2 sandwiched between few-layer hBN. **c,** Reflectance contrast (RC) spectrum of the sample measured at low temperature (4 K) showing three distinct absorption features at 1.937 eV, 2.004 eV and 2.113 eV for X_A, hIX and hX_B, respectively. The measured linewidths for X_A, hIX, and hX_B are 20, 23 and 64 meV, respectively. RC is calculated using the formula in the top-right corner of the graph. **d,** Sketch of the conduction and valence bands in two adjacent layers of MoS_2, displaying the allowed optical transitions of A and B direct intralayer excitons (X_A and X_B) and interlayer excitons (IX) for spin-up states (black lines) at the K point in the bilayer momentum space. IX hybridizes with X_B through the hole tunnelling between the two layers (red dashed arrow). At the K' point of the bilayer Brillouin zone, the same configuration applies for the states with the opposite spins. **e,** RC spectra of excitons in BL MoS_2 detected in two circular polarizations in an out-of-plane magnetic field of 8 T at T=4 K. Zeeman shifts of opposite signs are observed for X_A and hIX. The absorption peak of the charged intralayer exciton (X_A^*) shows near unity circular polarization.

approach allows realization of uniform samples suitable for the observation of macroscopic many-body phenomena [38]. Interlayer excitons unique to bilayer MoS_2 possess a large oscillator strength, comparable to that of the intralayer exciton, arising from interlayer hybridization of valence band states, aided by a favourable orbital overlap and a relatively small spin-orbit splitting among semiconducting TMDs [12]. Such hybridized interlayer excitons (hIX) are highly tunable using out-of-plane electric field [11, 15] and their valley degree of freedom persists up to room temperature [16].

Here we use hIXs in bilayer MoS_2 to realize highly nonlinear excitonic and dipolaritonic effects. We unravel a previously unexplored interaction regime involving intra- and interlayer excitons stemming from the fermionic nature of the charge carriers in a valence band shared between different excitonic species. This regime, accessible using broadband excitation resonant with both hIX and intralayer exciton transitions, provides strong (up to 10 times) enhancement of the exciton nonlinearity, already enhanced by up to 8 times in MoS_2 bilayers compared with monolayers. We support our experimental findings with microscopic theory, analysing the excitonic many-body physics and the cross-interactions and introducing the nonlinear mechanisms of the hole crowding.

Our heterostructure samples consists of a MoS_2 bilayer (BL) sandwiched between hBN and placed on a distributed Bragg reflector (DBR). Fig. 1a shows a bright field microscope image of the encapsulated BL MoS_2. A sketch of the side view of the device is displayed in Fig. 1b. The reflectance contrast (RC) spectrum of the studied MoS_2 bilayer, displayed in Fig. 1c, shows three peaks: the intralayer neutral excitons X_A at at 1.937 eV (see Fig. 1d), hybridized interlayer exciton hIX at 2.004 eV and hybridized B-exciton at 2.113 eV. Due to the quantum tunnelling of holes, B-excitons hybridize with an interlayer exciton (IX) (Fig. 1d), which is a direct transition in the bilayer momentum space [12]. The ratio of the integrated intensities of X_A and hIX is 4.5. Based on these data, we estimate the electron-hole separation $d = 0.55$ nm (see details in Supplementary Note S1) in agreement

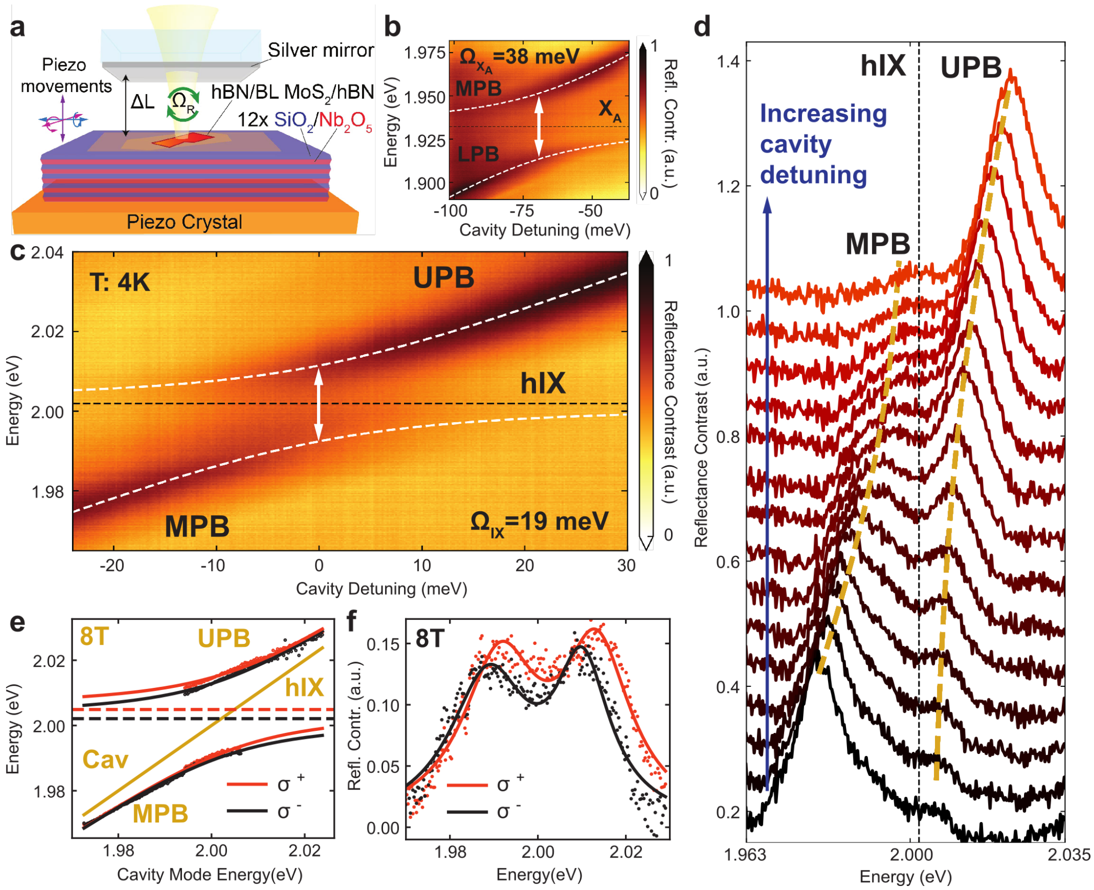

FIG. 2. **Strong exciton-photon coupling in MoS_2 bilayers.** **a,** Schematics of the tunable open microcavity composed of a bottom DBR and a top semi-transparent silver mirror. **b, c,** Low temperature (4K) RC spectra measured as a function of the cavity-exciton detuning ($\Delta = E_{\text{cav}} - E_{\text{exc}}$) for cavity scans across **b** X_A and **c** hIX energies. White dotted lines show the fitting obtained using the coupled-oscillator model providing the Rabi splittings $\Omega_{\text{hiX}} = 19$ meV and $\Omega_{X_A} = 38$ meV. **d,** RC spectra measured for the cavity-exciton detunings in the vicinity of the anticrossing between hIX and the cavity mode. **e,** Dipolariton dispersion measured with circularly polarized detection for 8 T magnetic field. The orange and black solid curves are the coupled oscillator model fits for σ^+ and σ^- detection, respectively. The positions of the Zeeman-split hIX peaks are shown by dashed lines. **f,** σ^+ (orange) and σ^- (black) RC spectra measured at 8 T at the hIX-cavity anticrossing. Fitting with two Lorentzians (solid lines) is shown.

with previous studies [16]. We further confirm the nature of the hIX states by placing the BL MoS_2 in magnetic field where the valley degeneracy is lifted (Fig. 1e). In agreement with recent studies [15, 39], we measure a Zeeman splitting with an opposite sign and larger magnitude in hIX compared with X_A (-3.5 versus 1.5 meV).

We study the strong coupling regime in a tunable planar microcavity (Fig. 2a) formed by a silver mirror and a planar DBR [7]. RC scans as a function of the cavity mode detuning $\Delta = E_{cav} - E_{exc}$, where E_{cav} and E_{exc} are the cavity mode and the corresponding exciton energy, respectively, are shown in Fig. 2c,d. Characteristic anticrossings of the cavity mode with X_A and hIX are observed, resulting in lower, middle and upper polariton branches (LPB, MPB, and UPB, respectively). The extracted Rabi splittings are $\Omega_{\mathrm{X_A}} = 38$ meV for X_A and $\Omega_{\mathrm{hIX}} = 19$ meV for hIX (Supplementary Note S2). Fig. 2d shows the RC spectra in the vicinity of the anticrossing with hIX, providing a more detailed view of the formation of the MPB and UPB. The intensity of the polariton peaks is relatively low for the states with a high exciton fraction at positive (negative) cavity detunings for the MPB (UPB). As the Rabi splitting scales as a square root of the oscillator strength, the ratio $\Omega_{\mathrm{X_A}}/\Omega_{\mathrm{hIX}} = 2$ is in a good agreement with the RC data for integrated intensities of X_A and hIX. From the Rabi splitting ratio we can estimate the tunneling constant J leading to the exciton hybridization. The corresponding coefficient is $J = 48$ meV (see Supplementary Note S1 for details), matching the density functional theory predictions [12]. In polarization-resolved cavity scans in an out-of-plane magnetic field (Fig. 2e,f), similarly to hIX behaviour, we observe opposite and larger Zeeman splitting for dipolaritons relative to the intralayer polaritons (see Supplementary Figure S4). Chiral dipolariton states are observed distinguished by their opposite circular polarization (Fig. 2f).

We investigate the nonlinear response of X_A and hIX in the bare BL flake as a function of the laser power using both narrow band (NB, full-width at half maximum, FWHM=28nm) and broad band (BB, FWHM=50 nm) pulsed excitation (see Methods). Our resonant pump-probe experiments have confirmed that the lifetimes of the hIX and X_A states are considerably longer than the pulse duration of ≈ 150 fs (Supplementary Note S3). Measured RC spectra are shown in Fig. 3a,b for the NB and in Fig. 3c for BB excitation. In the NB case, the excitation was tuned to excite either X_A or hIX independently, while in the BB case, both resonances were excited simultaneously.

As seen in Figs. 3a,b both X_A and hIX spectra behave similarly upon increasing the power of the NB excitation: a blueshift of several meV is observed, accompanied by the peak broadening and bleaching. For the BB excitation, however, a different nonlinear behaviour is observed as shown in Fig. 3c: the broadening and complete suppression of the hIX peak is observed at much lower powers, accompanied by a redshift. This is in contrast to X_A, whose behaviour is similar under the two excitation regimes.

The resulting energy shifts, peak linewidths and intensities are shown in Fig. 3d,e as a function of the exciton density (see details in Supplementary Note S4 and S6). Fig. 3d quantifies the trends observed in Figs. 3a,b showing for the BB excitation an abrupt bleaching of the hIX peak above the hIX density 5×10^3 μm^{-2} accompanied by a redshift of $\approx$ 4 meV and a 12 meV broadening. For the NB case, a similar decrease in peak intensity is observed only around 4×10^4 μm^{-2}, accompanied with a peak blueshift of $\approx$ 7 meV and a broadening exceeding 15 meV. In Fig. 3e, however, it is apparent that the observed behaviour under the two excitation regimes is similar for X_A. A similar blueshift, broadening and saturation are observed at slightly higher densities compared to the hIX under the NB excitation (Supplementary Note S5). We also find that due to the increased excitonic Bohr radius, the onset

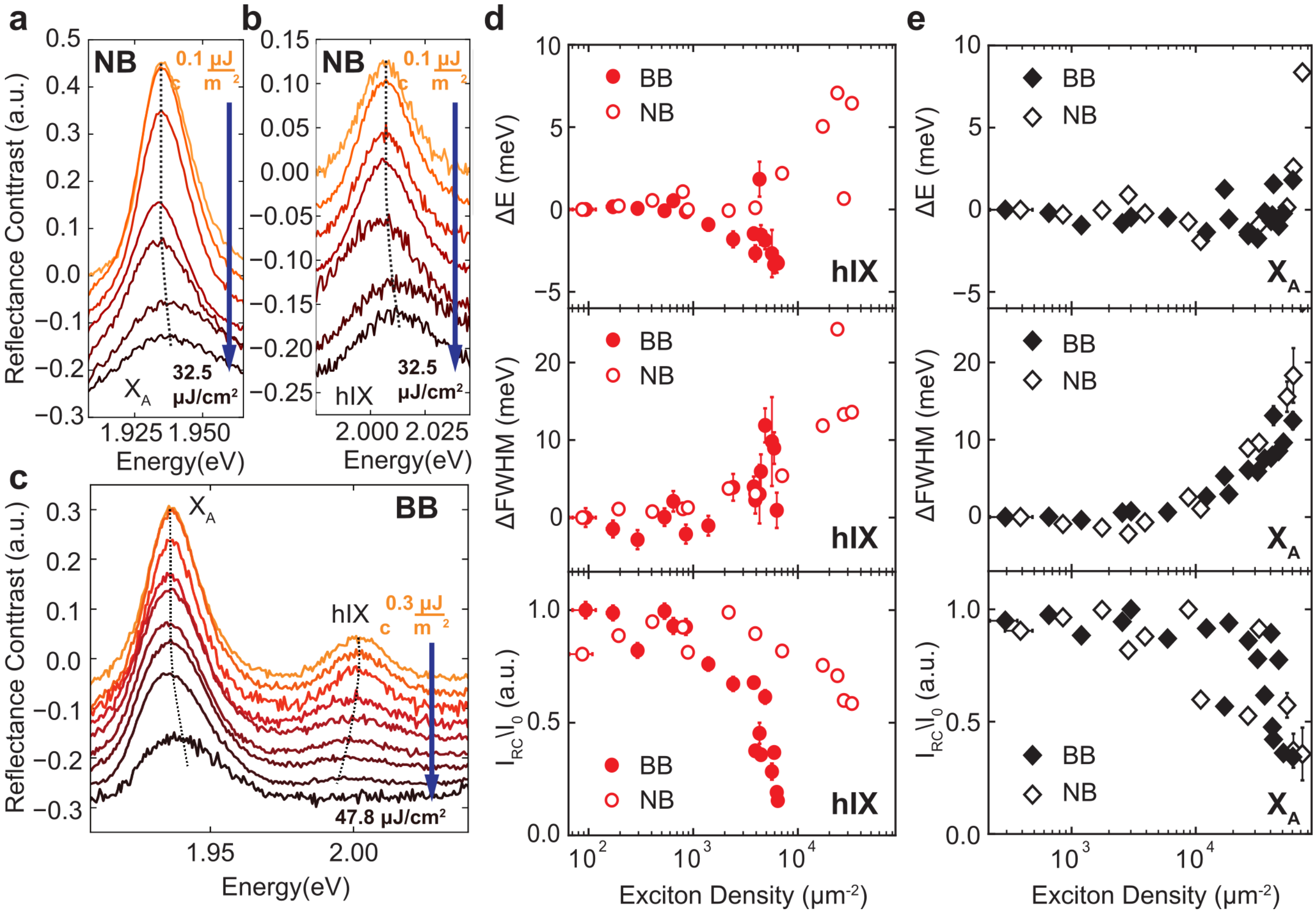

FIG. 3. **Exciton nonlinearity in MoS_2 bilayers.** **a, b, c,** RC spectra measured with the NB (FWHM=28nm) excitation for the X_A (**a**) and hIX (**b**), and with the BB (FWHM=50nm) excitation (**c**) at different fluences. The dashed curves are guide for the eye. **d, e,** The energy shift ΔE (top), linewidth variation ΔFWHM (middle) and normalized integrated intensity (bottom) as a function of the exciton density for the hIX (d) and X_A (e). Solid (open) symbols show the results for the BB (NB) excitation. For the normalized intensity we divide the intergrated intensity at each laser power by that at the maximum intensity.

of the nonlinear behaviour for X_A in bilayers occurs at a lower exciton density than for X_A in monolayers (Supplementary Note S7).

We develop a microscopic model to describe the contrasting phenomena under the NB and BB excitation. Under the NB excitation, either X_A or hIX excitons are created as sketched in Fig. 4a. In this case, nonlinearity arises from Coulomb exciton-exciton interactions causing the blueshift and dephasing [40]. For simplicity, in the main text we will use a Coulomb potential V_{Coul} combining the exchange and direct terms further detailed in Supplementary Note S8. We confirm (see Supplementary Note S8) that for the intralayer exciton-exciton interaction (X_A-X_A) the dominant nonlinear contribution comes from the Coulomb exchange processes, as in the monolayer case [40, 41], while for the hIX-hIX scattering the dominant contribution is from the direct Coulomb (dipole-dipole) interaction terms [19]. For both X_A and hIX, the Coulomb interaction is repulsive, and thus leads to the experimentally observed blueshifts. We find that for the modest electron-hole separation $d = 0.55$ nm in the bilayer, V_{Coul} is overall 2.3 times stronger for hIX compared with X_A.

Analysing the shapes of the reflectance spectra in the NB case, we note that they depend on the rates of radiative ($\Gamma_{\rm R}$) and non-radiative ($\Gamma_{\rm NR}$) processes. The area under RC curves is described by the ratio $\Gamma_{\rm R}/(\Gamma_{\rm R}+\Gamma_{\rm NR})$. This ratio changes under the increased excitation if the rates depend on the exciton densities. Specifically, we account for the scattering-induced non-radiative processes that microscopically scale as $\Gamma_{\rm NR} \propto |V_{\rm Coul}|^2 n$, i.e. depend on the absolute value of the combined matrix elements for the Coulomb interactions and the exciton density n [40]. This process allows reproducing the RC behaviour and bleaching at increasing pump intensity. Moreover, it explains stronger nonlinearity for X_A in bilayers compared to monolayers. Namely, the scattering scales with the exciton Bohr radius, $V_{\rm Coul} \propto \alpha$, which is larger in the bilayers due to the enhanced screening (Supplementary Note S8).

In the BB case, both X_A and hIX excitons are generated simultaneously, and together with intraspecies scattering (X_A-X_A and hIX-hIX), interspecies scattering (X_A-hIX) occurs, similarly to the direct-indirect exciton Coulomb scattering in

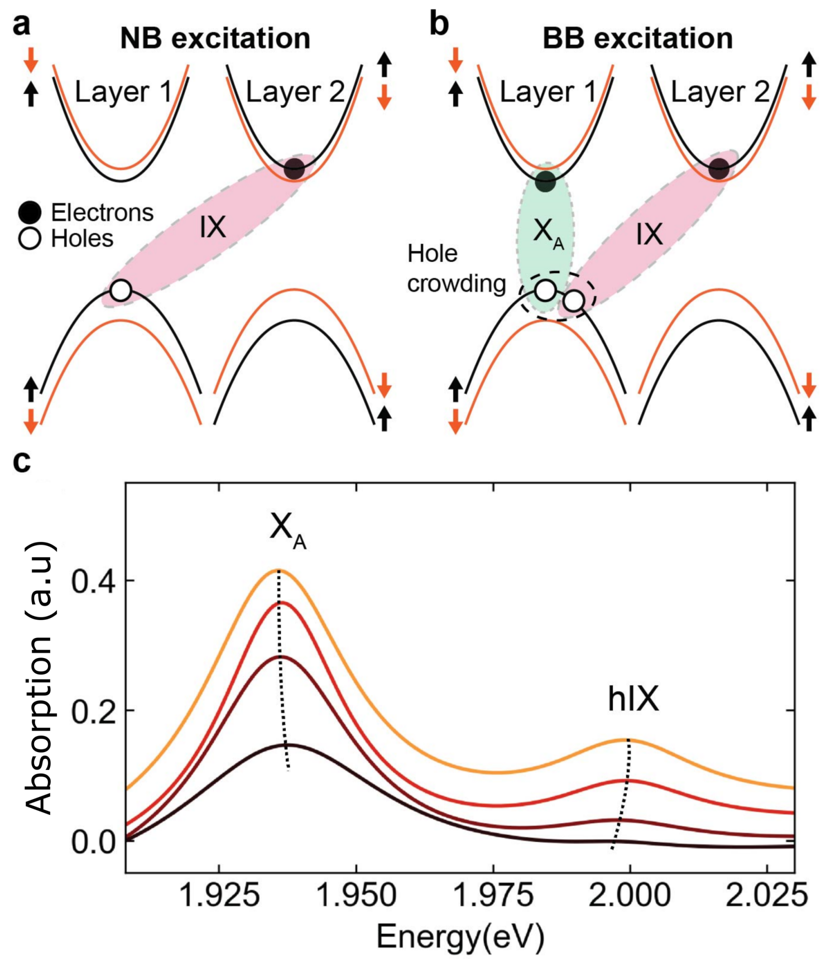

FIG. 4. **Theoretical model for nonlinear optical response in MoS_2 bilayers. a, b,** Schematic diagram showing exciton generation under the NB (a) and BB (b) excitation. In (a) only generation of hIX is shown. In (b), the holes of the two excitonic species share the same valence band. **c,** Theoretically calculated absorption spectra for the BB excitation case (see Supplementary Note S8), providing qualitative agreement with the experiment. The dashed black curves are guides for the eye.

double quantum wells [42]. Since X_A and hIX are formed by the holes from the same valence band (Fig. 4a), an additional contribution arises from the phase space filling, i.e. the commutation relations for the excitons (composite bosons) start to deviate from the ideal weak-density limit once more particles are created [43]. For particles of the same flavour, the phase space filling enables nonlinear saturation effects in the strong coupling regime, similar to polariton saturation observed in [29].

However, in the presence of several exciton species, we reveal a distinct phase space filling mechanism which we term the *hole crowding*. Crucially, we observe that the commutator of the X_A annihilation operator ($\hat{X}$) and hIX creation operator ($\hat{I}^\dagger$) is non-zero, $[\hat{X}(\mathbf{p}), \hat{I}^\dagger(\mathbf{q})] = -\hat{B}_{\mathbf{p},\mathbf{q}}$. Here $\mathbf{p}$, $\mathbf{q}$ are exciton momenta and $\hat{B}_{\mathbf{p},\mathbf{q}}$ is an operator denoting the deviation from the ideal commuting case ($\hat{B}_{\mathbf{p},\mathbf{q}} = 0$) of distinct bosons where holes do not compete for the valence band space.

This statistical property of modes that share a hole has profound consequences for the nonlinear response. Namely, the total energy is evaluated as an expectation value over a many-body state with both X_A and hIX excitons, $|N_{\mathrm{X}}, N_{\mathrm{hIX}}\rangle := (\prod_{\mathbf{p}}^{N_{\mathrm{X}}} \hat{X}^\dagger)(\prod_{\mathbf{q}}^{N_{\mathrm{hIX}}} \hat{I}^\dagger)|\Omega_{max}\rangle$, where N_{X} and N_{hIX} particles are created from the ground state $|\Omega_{max}\rangle$. If the excitonic modes are independent, the contributions from X_A and hIX simply add up. However, the hole coexistence in the valence band induces the excitonic interspecies scattering. The phase space filling combined with the Coulomb energy correction leads to a negative nonlinear energy contribution. This nonlinear term scales as $\Delta E_{\mathrm{hIX}} = -\eta\sqrt{n_{\mathrm{X}} n_{\mathrm{hIX}}}$, where $\eta > 0$ is a coefficient defined by the Coulomb energy and Bohr radii and $n_{\mathrm{X,hIX}}$ are the exciton densities (see Supplementary Note S9). This nonlinearity also modifies the non-radiative processes leading to substantial broadening for the hIX states.

According to this analysis, the effect of the BB excitation should be most pronounced for hIX. In addition to the possible hIX-hIX scattering (similar to that occurring under the NB excitation), much stronger X_A absorption leads to the phase space filling in the valence band. Such hole crowding introduces additional scattering channels for hIX and leads to its RC spectra bleaching at lower hIX exciton densities. On the other hand, as only relatively small hIX densities can be generated, both the NB and BB excitation cases should produce similar results for

X_A. Using the estimated nonlinear coefficients caused by the hole crowding, we model the RC in the BB regime and qualitatively reproduce the strong bleaching and redshift for hIX at the increased density.

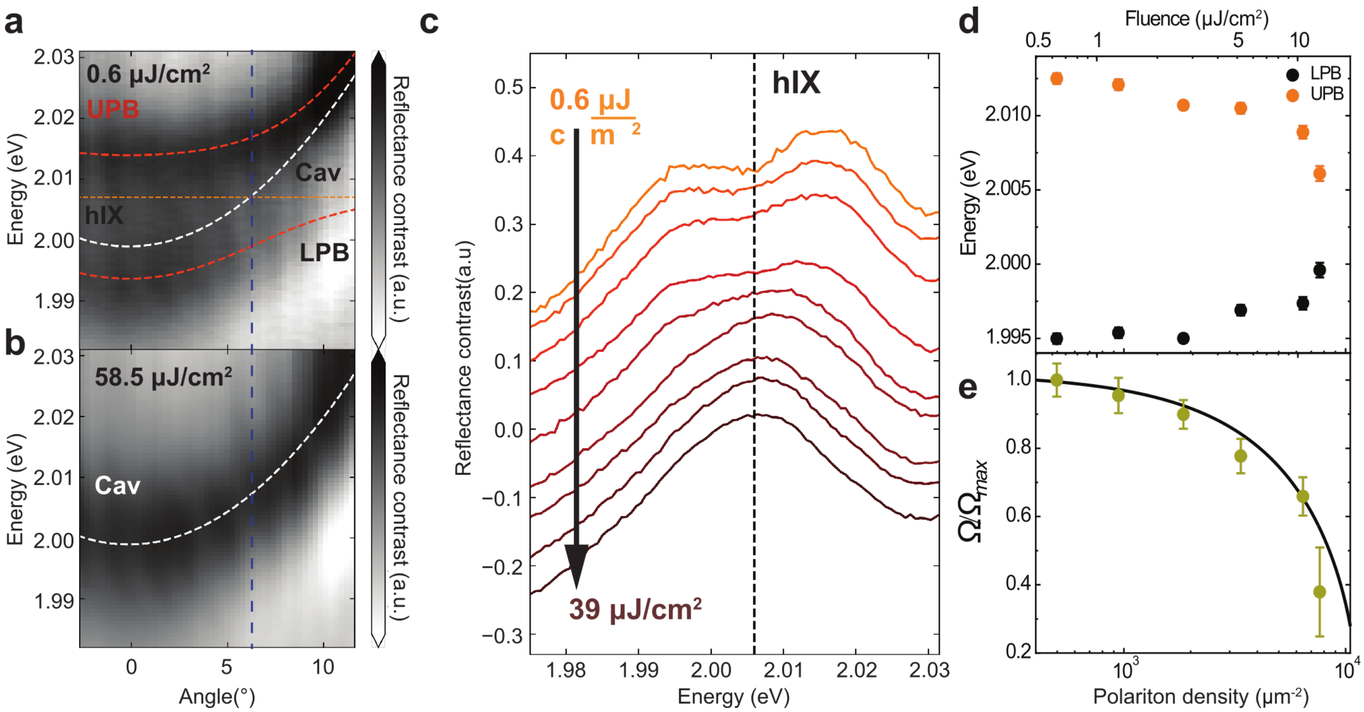

FIG. 5. **Nonlinear behaviour of dipolaritons. a, b,** Reflectance contrast spectra measured at different laser fluences for the MoS_2 bilayer placed in a monolithic cavity. (a) The low fluence case (0.6 μJ cm^{-2}). A clear anticrossing at 6.5°is observed. Dashed red lines show the results of the fitting using a coupled oscillator model, with two polariton branches LPB and UPB formed. White and orange lines show the energies of the uncoupled cavity mode and hIX state, respectively. The vertical line marks the anticrossing angle. (b) The high fluence case (58.5 μJ cm^{-2}). A complete collapse of the strong coupling regime is observed, with the disappearance of the anticrossing and transition into the weak coupling regime. **c,** RC spectra measured at the anticrossing at 6.5° as a function of the laser fluence. **d,** Measured UPB and LPB peak energies at 6.5° as a function of the laser fluence (see top axis) and the corresponding polariton density (bottom axis). **e,** Symbols show the Rabi splittings normalized by the Rabi splitting measured at the lowest power (Ω/Ω_{max}) as deduced from **d,**. The line shows the fitting using our theoretical model (Supplementary Note S8).

We investigate nonlinear properties of dipolar polaritons in a monolithic (fixed-length) cavity created by a silver mirror on top of a PMMA spacer (245 nm thick) covering the hBN-encapsulated MoS_2 homobilayer placed on the DBR. The cavity mode energy can be tuned by varying the angle of observation (0 degrees corresponds to normal incidence). We use a microscopy setup optimized for Fourier-plane imaging, thus allowing simultaneous detection of reflectivity spectra in a range of angles as shown in Fig.5(a) displaying the measured polariton dispersion. In this experiment, the cavity mode is tuned around hIX and only two polariton branches LPB and UPB are observed at low fluence of 0.6 μJ cm^{-2} with a characteristic Rabi splitting of 17.5 meV. In Fig.5(b), at an increased fluence of 58.5 μJ cm^{-2}, only a weakly coupled cavity mode is visible.

Fig.5(c) shows RC spectra taken at $\sim 6.5°$ around the anticrossing at different laser fluences. The collapse of the two polariton peaks into one peak signifying the transition to the weak coupling regime is observed above 25 μJ cm^{-2}. The LPB and UPB energies extracted using the coupled oscillator model (Supplementary Figure S5) are shown in Fig.5(d). As the polariton density is increased, the LPB and UPB approach each other almost symmetrically, converging to the exciton energy. The corresponding normalized Rabi splitting (Ω/Ω_{max}, where Ω_{max} is measured at low fluence) are shown in Fig.5(d,e) as a function of the total polariton density.

In this experiment, the cavity mode is considerably above the X_A energy, which therefore is not coupled to the cavity. Hence, the extracted Rabi splittings are fitted with a theoretically predicted trend of Ω for the NB excitation regime (Supplementary Note S8). A nonlinear polariton coefficient $\beta = 0.86$ μeVμm^2 is extracted by differentiating the fitted function with respect to the polariton density. Comparing our results to X_A intralayer-exciton-polaritons in monolayers in similar cavities [14], we observe that the nonlinearity coefficient for dipolar interlayer polaritons is about an order of magnitude larger. This is in a good agreement with the theoretically predicted intrinsic nonlinearity of hybridized interlayer polaritons (Supplementary Note S8), and with our experimental data comparing hIX and monolayer X_A outside the cavity (Supplementary Note S7).

In summary, we report the nonlinear exciton and exciton-polariton behaviour in MoS_2 homobilayers, a unique system where hybridized interlayer exciton states can be realized having a large oscillator strength. We find that nonlinearity in MoS_2 bilayers can be enhanced when both the intralayer and interlayer states are excited simultaneously, the regime that qualitatively changes the exciton-exciton interaction through the hole crowiding effect introduced theoretically in our work. In this broad-band excitation regime, the bleaching of the hIX absorption occurs at 8 times lower hIX densities compared to the case when the interlayer excitons are generated on their own. In addition to this, we find that the dipolar nature of hIX states in MoS_2 homobilayers already results in 10 times stronger nonlinearity compared with the intralayer excitons in MoS_2 monolayers. Thus, we report on an overall enhancement of the nonlinearity by nearly two orders of magnitude. Thanks to the large oscillator strength, hIX can enter the strong coupling regime in MoS_2 bilayers placed in microcavities, as realized in our work. Similarly to hIX states themselves, dipolar polaritons also show 10 times stronger nonlinearity compared with exciton-polaritons in MoS_2 monolayers. We expect that in microcavities where the cavity mode is coupled to both hIX and X_A in MoS_2 bilayers, and the excitation similar to the broad-band regime can thus be realized, the nonlinear polariton coefficient will be dramatically enhanced owing to the hole crowding effect, allowing highly nonlinear polariton system to be realized. We thus predict that MoS_2 bilayers will be an attractive platform for realization of quantum-correlated polaritons with applications in polariton logic networks [20] and polariton blockade [21, 22].

METHODS

The hBN/MoS_2/hBN heterostructures were assembled using a PDMS polymer stamp method. The PMMA spacer for the monolithic cavity was deposited using a spin-coating technique, while a silver mirror of 45 nm was thermally evaporated on top of it.

Broad-band excitation was used to measure the reflectance contrast (RC) spectra of the devices at cryogenic temperatures (4K), defined as RC $= (R_{\mathrm{sub}} - R_{\mathrm{BL}})/R_{\mathrm{sub}}$, where R_{sub} and R_{BL} are the substrate and MoS_2 bilayer reflectivity, respectively. For the magnetic field studies the same RC measurements were performed using unpolarized light in excitation with polarizers, $\lambda/4$ polarizers and $\lambda/2$ waveplates in collection, to resolve σ^+ and σ^- polarization. The low temperature measurements using the tunable cavity were carried out in a liquid helium bath cryostat (T=4.2K) equipped with a superconducting magnet and free beam optical access. We used a white light LED as a source. RC spectra were measured at each ΔL and are integrated over the angles within 5 degrees from normal incidence. The RC spectra measured in the cavity are fitted using Lorenzians. The peak positions are then used to fit to a coupled oscillator model, producing the Rabi splitting and the exciton and cavity mode energies.

The measurements on the monolithic cavity were performed in a closed loop helium flow cryostat (T=6K). For the power-dependent RC experiments, we used super-continuum radiation produced by 100 fs Ti:Sapphire laser pulses at 2 kHz repetition rate at 1.55 eV propagating through a thin sapphire crystal. The supercontinuun radiation was then filtered to produce the desired narrow-band excitation.

All the exciton and polariton densities were calculated following the procedure introduced by L. Zhang et al. [14], taking into account the spectral overlap of the spectrum of the excitation laser and the investigated exciton peak (see further details in Supplementary Note S4).

ACKNOWLEDGEMENTS

CL, AG, TPL, SR and AIT acknowledge financial support of the European Graphene Flagship Project under grant agreement 881603 and EPSRC grants EP/V006975/1, EP/V026496/1, EP/V034804/1 and EP/S030751/1. TPL acknowledges financial support from the EPSRC Doctoral Prize Fellowship scheme. CT, SDC and GC acknowledge support by the European Union Horizon 2020 Programme under Grant Agreement 881603 Graphene Core 3. AG and GC acknowledge support by the European Union Marie Sklodowska-Curie Actions project ENOSIS H2020-MSCA-IF-2020-101029644. PC, RJ and DGL thank EPSRC Programme Grant 'Hybrid Polaritonics' (EP/M025330/1).

AUTHOR CONTRIBUTIONS

CL and SR fabricated and characterized hBN-encapsulated MoS_2 samples. KW and TT synthesized the high quality hBN. CL and AG designed the microcavity samples. PC, RJ, DGL fabricated the microcavity samples. CL, AG, CT, TL and SDC carried out optical spectroscopy experiments. SC and OK developed theory. AG calculated polariton densities. CL and AG analyzed the data with contribution from AIT, TL, SC, OK, CT, SDC and GC. CL, AG, SC, OK and AIT wrote the manuscript with contribution from all other co-authors. AIT, OK, DGL, GC managed various aspects of the project. AIT supervised the project.

DATA AVAILABILITY

The data that support the findings of this study are available from the corresponding author upon request.

* clouca1@sheffield.ac.uk

† armando.genco@polimi.it

‡ a.tartakovskii@sheffield.ac.uk

[1] H. Deng, H. Haug, and Y. Yamamoto, Exciton-polariton Bose-Einstein condensation, Reviews of Modern Physics **82**, 1489 (2010).

[2] J. Kasprzak *et al.*, Bose-Einstein condensation of exciton polaritons, Nature **443**, 409 (2006).

[3] S. Christopoulos *et al.*, Room-temperature polariton lasing in semiconductor microcavities, Physical Review Letters **98**, 126405 (2007).

[4] P. Bhattacharya *et al.*, Room temperature electrically injected polariton laser, Physical Review Letters **112**, 236802 (2014).

[5] A. Amo *et al.*, Collective fluid dynamics of a polariton condensate in a semiconductor microcavity, Nature **457**, 291 (2009).

[6] X. Liu, T. Galfsky, Z. Sun, F. Xia, E. C. Lin, Y. H. Lee, S. Kéna-Cohen, and V. M. Menon, Strong light-matter coupling in two-dimensional atomic crystals, Nature Photonics **9**, 30 (2014).

[7] S. Dufferwiel, S. Schwarz, F. Withers, A. A. Trichet, F. Li, M. Sich, O. Del Pozo-Zamudio, C. Clark, A. Nalitov, D. D. Solnyshkov, G. Malpuech, K. S. Novoselov, J. M. Smith, M. S. Skolnick, D. N. Krizhanovskii, and A. I. Tartakovskii, Exciton-polaritons in van der Waals heterostructures embedded in tunable microcavities, Nature Communications **6**, 1 (2015).

[8] N. Lundt, A. Maryński, E. Cherotchenko, A. Pant, X. Fan, S. Tongay, G. Sek, A. V. Kavokin, S. Höfling, and C. Schneider, Monolayered $MoSe_2$: A candidate for room temperature polaritonics, 2D Materials **4** (2017).

[9] M. Sidler, P. Back, O. Cotlet, A. Srivastava, T. Fink, M. Kroner, E. Demler, and A. Imamoglu, Fermi polaron-polaritons in charge-tunable atomically thin semiconductors, Nature Physics **13**, 255 (2017).

[10] S. Dufferwiel, T. P. Lyons, D. D. Solnyshkov, A. A. Trichet, F. Withers, S. Schwarz, G. Malpuech, J. M. Smith, K. S. Novoselov, M. S. Skolnick, D. N. Krizhanovskii, and A. I. Tartakovskii, Valley-addressable polaritons in atomically thin semiconductors, Nature Photonics **11**, 497 (2017).

[11] N. Leisgang, S. Shree, I. Paradisanos, L. Sponfeldner, C. Robert, D. Lagarde, A. Balocchi, K. Watanabe, T. Taniguchi, X. Marie, *et al.*, Giant stark splitting of an exciton in bilayer mos2, Nature Nanotechnology **15**, 901 (2020).

[12] I. C. Gerber, E. Courtade, S. Shree, C. Robert, T. Taniguchi, K. Watanabe, A. Balocchi, P. Renucci, D. Lagarde, X. Marie, and B. Urbaszek, Interlayer excitons in bilayer MoS_2 with strong oscillator strength up to room temperature, Physical Review B **99**, 1 (2019).

[13] N. P. Wilson, W. Yao, J. Shan, X. XuExcitons and emergent quantum phenomena in stacked 2D semiconductors Nature **599**, 383-392 (2021).

[14] L. Zhang, F. Wu, S. Hou, Z. Zhang, Y.-H. Chou, K. Watanabe, T. Taniguchi, S. R. Forrest, and H. Deng, Van der waals heterostructure polaritons with moiré-induced nonlinearity, Nature **591**, 61 (2021).

[15] E. Lorchat, M. Selig, F. Katsch, K. Yumigeta, S. Tongay, A. Knorr, C. Schneider, and S. Höfling, Excitons in bilayer mos 2 displaying a colossal electric field splitting and tunable magnetic response, Physical Review Letters **126**, 037401 (2021).

[16] N. Peimyoo, T. Deilmann, F. Withers, J. Escolar, D. Nutting, T. Taniguchi, K. Watanabe, A. Taghizadeh, M. F. Craciun, K. S. Thygesen, and S. Russo, Electrical tuning of optically active interlayer excitons in bilayer MoS_2, Nature Nanotechnology **16**, 888 (2021).

[17] P. Cristofolini, G. Christmann, S. I. Tsintzos, G. Deligeorgis, G. Konstantinidis, Z. Hatzopoulos, P. G. Savvidis, and J. J. Baumberg, Coupling quantum tunneling with cavity photons Science **336**, 704-707 (2012).

[18] E. Togan, H.-T. Lim, S. Faelt, W. Wegscheider, and A. Imamoglu, Enhanced interactions between dipolar polaritons, Phys. Rev. Lett. **121**, 227402 (2018).

[19] O. Kyriienko, E. B. Magnusson, and I. A. Shelykh, Spin dynamics of cold exciton condensates, Phys. Rev. B **86**, 115324 (2012).

[20] N. G. Berloff, M. Silva, K. Kalinin, A. Askitopoulos, J. D. Töpfer, P. Cilibrizzi, W. Langbein, and P. G. Lagoudakis, Realizing the classical xy hamiltonian in polariton simulators, Nature Materials **16**, 1120 (2017).

[21] A. Delteil, T. Fink, A. Schade, S. Höfling, C. Schneider, and A. İmamoğlu, Towards polariton blockade of confined exciton–polaritons, Nature Materials **18**, 219 (2019).

[22] O. Kyriienko, D. Krizhanovskii, and I. Shelykh, Nonlinear quantum optics with trion polaritons in 2d monolayers: conventional and unconventional photon blockade, Physical Review Letters **125**, 197402 (2020).

[23] G. Wang, A. Chernikov, M. M. Glazov, T. F. Heinz, X. Marie, T. Amand, and B. Urbaszek, Colloquium: Excitons in atomically thin transition metal dichalcogenides, Reviews of Modern Physics **90**, 21001 (2018).

[24] T. P. Lyons, D. J. Gillard, C. Leblanc, J. Puebla, D. D. Solnyshkov, L. Klompmaker, I. A. Akimov, C. Louca, P. Muduli, A. Genco, M. Bayer, Y. Otani, G. Malpuech, and A. I. Tartakovskii, Giant effective Zeeman splitting in a monolayer semiconductor realized by spin-selective strong light-matter coupling, (2021).

[25] D. J. Gillard, A. Genco, S. Ahn, T. P. Lyons, K. Yeol Ma, A. R. Jang, T. Severs Millard, A. A. Trichet, R. Jayaprakash, K. Georgiou, D. G. Lidzey, J. M. Smith, H. Suk Shin, and A. I. Tartakovskii, Strong exciton-photon coupling in large area $MoSe_2$ and WSe_2 heterostructures fabricated from two-dimensional materials grown by chemical vapor deposition, 2D Materials **8** (2021).

[26] J. Gu, B. Chakraborty, M. Khatoniar, and V. M. Menon, A room-temperature polariton light-emitting diode based on monolayer WS_2, Nature Nanotechnology **14**, 1024 (2019).

[27] N. Lundt, Ł. Dusanowski, E. Sedov, P. Stepanov, M. M. Glazov, S. Klembt, M. Klaas, J. Beierlein, Y. Qin, S. Tongay, *et al.*, Optical valley hall effect for highly valley-coherent exciton-polaritons in an atomically thin semiconductor, Nature Nanotechnology **14**, 770 (2019).

[28] L. B. Tan, O. Cotlet, A. Bergschneider, R. Schmidt, P. Back, Y. Shimazaki, M. Kroner, and A. İmamoğlu, Interacting polaron-polaritons, Physical Review X **10**, 021011 (2020).

[29] R. P. A. Emmanuele *et al.*, Highly nonlinear trion-polaritons in a monolayer semiconductor, Nature Communications **11**, 3589 (2020).

[30] J. Gu, V. Walther, L. Waldecker, D. Rhodes, A. Raja, J. C. Hone, T. F. Heinz, S. Kéna-Cohen, T. Pohl, and V. M. Menon, Enhanced nonlinear interaction of polaritons via excitonic Rydberg states in monolayer WSe_2, Nature Communications **12** (2021).

[31] P. Rivera, H. Yu, K. L. Seyler, N. P. Wilson, W. Yao, and X. Xu, Interlayer valley excitons in heterobilayers of transition metal dichalcogenides, Nature Nanotechnology **13**, 1004 (2018).

[32] L. V. Butov, Condensation and pattern formation in cold exciton gases in coupled quantum wells, Journal of Physics: Condensed Matter **16**, R1577 (2004).

[33] C. Hubert, Y. Baruchi, Y. Mazuz-Harpaz, K. Cohen, K. Biermann, M. Lemeshko, K. West, L. Pfeiffer, R. Rapaport, and P. Santos, Attractive dipolar coupling between stacked exciton fluids, Phys. Rev. X **9**, 021026 (2019).

[34] L. Butov, A. Gossard, and D. Chemla, Macroscopically ordered state in an exciton system, Nature **418**, 751 (2002).

[35] A. Fox, D. Miller, G. Livescu, J. Cunningham, and W. Jan, Excitonic effects in coupled quantum wells, Physical Review B **44**, 6231 (1991).

[36] E. M. Alexeev, D. A. Ruiz-Tijerina, M. Danovich, M. J. Hamer, D. J. Terry, P. K. Nayak, S. Ahn, S. Pak, J. Lee, J. I. Sohn, *et al.*, Resonantly hybridized excitons in moiré superlattices in van der waals heterostructures, Nature **567**, 81 (2019).

[37] I. Paradisanos, S. Shree, A. George, N. Leisgang, C. Robert, K. Watanabe, T. Taniguchi, R. J. Warburton, A. Turchanin, X. Marie, *et al.*, Controlling interlayer excitons in mos2 layers grown by chemical vapor deposition, Nature Communications **11**, 1 (2020).

[38] A. Amo, D. Sanvitto, F. Laussy, D. Ballarini, E. d. Valle, M. Martin, A. Lemaitre, J. Bloch, D. Krizhanovskii, M. Skolnick, *et al.*, Collective fluid dynamics of a polariton condensate in a semiconductor microcavity, Nature **457**, 291 (2009).

[39] Z. Gong, G. B. Liu, H. Yu, D. Xiao, X. Cui, X. Xu, and W. Yao, Magnetoelectric effects and valley-controlled spin quantum gates in transition metal dichalcogenide bilayers, Nature Communications **4**, 1 (2013).

[40] D. Erkensten, S. Brem, and E. Malic, Exciton-exciton interaction in transition metal dichalcogenide monolayers and van der waals heterostructures, Phys. Rev. B **103**, 045426 (2021).

[41] V. Shahnazaryan, I. Iorsh, I. A. Shelykh, and O. Kyriienko, Exciton-exciton interaction in transition-metal dichalcogenide monolayers, Phys. Rev. B **96**, 115409 (2017).

[42] K. Kristinsson, O. Kyriienko, T. C. H. Liew, and I. A. Shelykh, Continuous terahertz emission from dipolaritons, Phys. Rev. B **88**, 245303 (2013).

[43] M. Combescot, O. Betbeder-Matibet, and F. Dubin, The many-body physics of composite bosons, Physics Reports **463**, 215 (2008).